Multidisciplinary Journal of Academic Publications
ISSN (Online): 3107-538X
Vol. 02, Issue 06, November-December 2026

INFLUENCE OF SINGLE-FIN LOCATION ON LONG-DURATION MELTING AND BUOYANCY-DRIVEN FLOW OF LAURIC ACID IN A VERTICAL RECTANGULAR ENCLOSURE

Amirraza[1], Sachin Baraskar[2,]

Department of Mechanical Engineering, Sri Satya Sai University of Technology & Medical Sciences, Sehore 466001, Madhya Pradesh, India[1]

Department of Mechanical Engineering, Sri Satya Sai University of Technology & Medical Sciences, Sehore 466001, Madhya Pradesh, India[2]

Highlights

- Long-duration (175 min) charging of lauric acid with a single fin at two heights.
- Mid-height fin splits the melt into two cells and keeps the lower half active.
- Time to 70% melting cut by about 31% (mid-height fin) and 16% (upper fin).
- Neumann conduction reference isolates the convective share of melting.
- A fin should feed heat where buoyant flow arrives last: the lower enclosure.

ABSTRACT

Fins are the cheapest way to speed up charging of latent heat stores, but in a side-heated enclosure a fin also reorganises the buoyancy-driven flow of the melt, so its height matters as much as its size. This study examines how the height of a single horizontal aluminium fin changes the full charging history of lauric acid in a 50 mm × 120 mm vertical enclosure whose side wall is held at 70 °C. Two-dimensional transient simulations with the enthalpy–porosity method and the Boussinesq approximation were verified by a mesh study and validated against published single-fin experiments. Melting over 175 min was compared for an enclosure without a fin and with a fin at dimensionless heights of 0.50 and 0.80, and the melt fractions were interpreted against a one-dimensional Neumann conduction solution. All

cases pass from a conduction-dominated start to convection-dominated melting in which the melt stratifies and the last solid is left at the bottom, away from the heated wall. A mid-height fin divided the melt into two convection cells and sustained circulation in the lower half; it melted about 99% of the PCM in 175 min, against about 90% for the upper fin and 71% without a fin. Interpolated times to 70% melting were shorter by roughly 31% and 16%, respectively, and by 175 min the melt fraction was 2.6 and 2.4 times the conduction-only value, compared with 1.9 without a fin. A fin placed high in the enclosure mostly heats liquid that is already stratified. Fins in side-heated stores should therefore be positioned to supply heat to the lower region that natural convection reaches last.

Keywords: *Phase change material[1]; Latent heat thermal energy storage[2]; Fin location[3]; Natural convection[4]; Thermal stratification[5]; Enthalpy–porosity method[6]*

Nomenclature

A_{mush}	mushy-zone constant, kg m^{-3} s^{-1}
c_p	specific heat, J kg^{-1} K^{-1}
d	height of the lower fin surface above the bottom wall, m
d_f	dimensionless fin location, d/H_c
E	convective enhancement ratio, $\lambda_{avg}/\lambda_{cond}$
Fo	Fourier number, $\alpha t/L_c^2$
H	specific enthalpy, J kg^{-1}
H_c, L_c	enclosure height and width, m
k	thermal conductivity, W m^{-1} K^{-1}
L	latent heat of fusion, J kg^{-1}
L_f, t_f	fin length and thickness, m
s	conduction melt-front position, m
Ste	Stefan number
T	temperature, °C

MJAP

T_i, T_w	initial and heated-wall temperatures, °C
T_s, T_l	solidus and liquidus temperatures, °C
t	time, s or min
t_{50}, t_{70}	time to reach 50% and 70% melt fraction, min
V	velocity vector, m s^{-1}
α	thermal diffusivity of the liquid, m^2 s^{-1}
β	thermal expansion coefficient, K^{-1}
λ	liquid fraction
λ_{avg}, λ_{cond}	enclosure-averaged and conduction-only melt fractions
ζ	Neumann similarity constant
μ, ρ	dynamic viscosity (Pa s) and density (kg m^{-3})

1. INTRODUCTION

Latent heat thermal energy storage (LHTES) stores heat in the solid–liquid transition of a phase change material (PCM). Because the transition occurs over a narrow temperature range, an LHTES unit holds several times more energy per unit volume than a sensible store operating over the same temperature swing, which makes it attractive for solar water heating, building envelopes and the recovery of low-grade waste heat [1–3]. Organic PCMs such as paraffins and fatty acids melt congruently, do not supercool appreciably and remain stable over thousands of cycles, but their thermal conductivity is only about 0.15–0.4 W m^{-1} K^{-1} [4, 5]. Charging and discharging are therefore slow, and the achievable power, rather than the storage capacity, often limits the design. Conductivity enhancement by nanoparticles, metal foams, expanded graphite, heat pipes and extended surfaces has been reviewed extensively [6–8]. Metallic fins remain the most practical option because they are inexpensive, durable and easily manufactured, and their effect depends on material, length, thickness, number, pitch and orientation [9–11]. In melting, however, a fin acts in two ways at once. It conducts heat from the wall into the PCM, but it also places a solid obstacle in the path of the buoyant boundary layer that develops along the heated wall. Sharifi et al. [12] showed that horizontal fins can suppress natural convection in an enclosure, and Stritih [13] found that fins shortened solidification much more than melting, precisely because melting is already assisted by convection.

In a vertical enclosure heated from one side, the melt that forms on the hot wall rises, spreads beneath the top wall and returns along the solid–liquid interface. The interface consequently tilts, the upper region melts first, and the

solid that remains near the bottom, far from the heated wall, dictates the total charging time [14, 15]. Scaling analysis identifies the successive conduction, transition and convection regimes of this process [16]. Experiments by Kamkari and Shokouhmand [17] with one and three horizontal partial fins in a lauric acid enclosure showed shorter melting times and higher heat-transfer rates as the number of fins increased, and enthalpy–porosity simulations have reproduced such experiments well [18]. Studies in annular and shell-and-tube units likewise show that the best number and placement of fins depend on the orientation of the convective flow [19–21].

Comparatively few studies isolate the height of a single fin. Huang et al. [22] varied the position of one fin in a rectangular enclosure and reported that both the melting rate and the dominant heat-transfer mode change with fin height. In a companion study [23], the present authors analysed the first two minutes of melting in a 40 mm × 60 mm enclosure and compared one and two fins at different heights; that work concentrated on how fins seed the initial melt layer. The present paper addresses the complementary question of what happens over the full charging period, when convection and stratification govern the melting. Its specific contributions are: (i) a validated simulation of 175 min of charging in the 50 mm × 120 mm experimental enclosure of Ref. [17] with no fin and with a single fin at $d_f = 0.50$ and 0.80; (ii) a combined reading of liquid-fraction contours and velocity fields that explains how fin height changes the convection cells and the stratification; and (iii) a comparison against a Neumann conduction reference that separates the contribution of convection from that of the added fin area and yields simple design metrics (t_{50}, t_{70} and the enhancement ratio E).

2. PROBLEM FORMULATION AND NUMERICAL METHOD

2.1. Physical model

The domain (Figure 1) is a vertical rectangular enclosure of width $L_c = 50$ mm and height $H_c = 120$ mm, matching the internal dimensions of the experimental cell of Kamkari and Shokouhmand [17]. One vertical wall is kept at $T_w = 70$ °C; the opposite wall and the horizontal walls are adiabatic. A horizontal aluminium fin, $L_f = 40$ mm long and $t_f = 5$ mm thick, is attached to the heated wall with its lower surface at height d, and its location is expressed as $d_f = d/H_c$. Three configurations are compared: no fin, $d_f = 0.50$ and $d_f = 0.80$. The PCM is lauric acid, initially solid at $T_i = 25$ °C. Its properties are listed in Table 1.

Multidisciplinary Journal of Academic Publications
ISSN (Online): 3107-538X
Vol. 02, Issue 06, November-December 2026

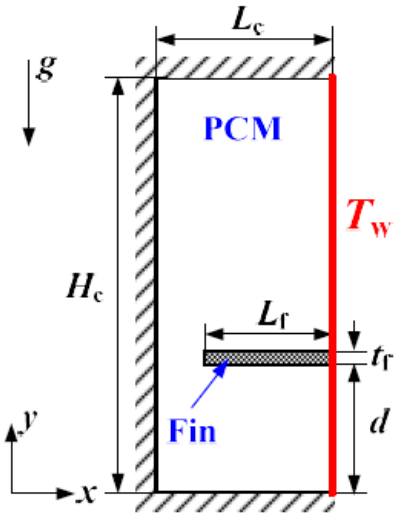


Figure 1: Schematic of the side-heated enclosure with a horizontal fin attached to the heated wall.

Table 1: Thermophysical properties of lauric acid used in the simulations.

Property	Value	Unit
Solidus / liquidus temperature, T_s / T_l	43.5 / 48.2	°C
Latent heat of fusion, L	187.21	kJ kg^{-1}
Specific heat, solid / liquid	2.18 / 2.39	kJ kg^{-1} K^{-1}
Density, solid / liquid	940 / 885	kg m^{-3}
Thermal conductivity, solid / liquid	0.16 / 0.14	W m^{-1} K^{-1}
Thermal expansion coefficient, β	8 × 10^{-4}	K^{-1}

2.2. Governing equations

The flow of the melt is taken as two-dimensional, laminar, Newtonian and incompressible, with buoyancy represented by the Boussinesq approximation. Viscous dissipation and the volume change on melting are neglected. Following the enthalpy–porosity approach [24, 25], one set of equations is solved over the solid, mushy and liquid regions:

$$\nabla \cdot V = 0 \tag{1}$$

$$\rho_l \left(\frac{\partial V}{\partial t} + (V \cdot \nabla)V\right) = -\nabla p + \mu \nabla^2 V + \rho_l g \beta (T - T_l) - A_{mush} \frac{(1-\lambda)^2}{\lambda^3 + \varepsilon} V \tag{2}$$

$$\frac{\partial (\rho H)}{\partial t} + \nabla \cdot (\rho V H) = \nabla \cdot (k \nabla T), \quad H = h_{ref} + \int_{T_{ref}}^{T} c_p dT + \lambda L \tag{3}$$

The last term of Eq. (2) is a Carman–Kozeny sink that drives the velocity to zero as the liquid fraction λ falls to zero; $\varepsilon = 10^{-3}$ avoids division by zero and $A_{mush} = 10^5$ kg m^{-3} s^{-1} (the solver default) was used. The liquid fraction varies linearly with temperature between the solidus and the liquidus,

$$\lambda = (T - T_s)/(T_l - T_s), \quad 0 \le \lambda \le 1 \tag{4}$$

and the progress of charging is measured by the area-averaged liquid fraction λ_{avg} of the PCM region (the fin area, 3.3% of the enclosure, is excluded).

2.3. Boundary conditions and solution procedure

No-slip conditions apply on all walls and on the fin. The heated wall and the fin root are held at 70 °C and the other walls are adiabatic; the fin is solved as a conducting aluminium zone coupled to the PCM. The equations were discretised with the finite-volume method in ANSYS Fluent 15.0 [26]. Pressure–velocity coupling used the SIMPLE algorithm [27] with PRESTO! pressure interpolation; momentum was discretised with the second-order upwind scheme and energy with the first-order upwind scheme. The time step was 0.1 s, with up to ten iterations per step and convergence criteria of 10^{-5}, 10^{-8} and 10^{-10} for the continuity, momentum and energy residuals, respectively.

2.4. Mesh independence and validation

Structured quadrilateral meshes of 3,515, 7,260, 16,527 and 29,628 cells, refined near the heated wall and around the fin, were compared for the finned enclosure at the same instant (Table 2, Figure 2). The liquid fraction changed by 2.1% between the two coarsest meshes, by 0.25% between the second and third, and was unchanged between the two finest; the 16,527-cell mesh was retained.

Table 2: Mesh-independence test (finned enclosure, same physical time).

Mesh	Cells	λ_{avg}	Change
M1	3,515	0.392	–
M2	7,260	0.400	2.1%
M3 (selected)	16,527	0.401	0.25%
M4	29,628	0.401	0.0%

Multidisciplinary Journal of Academic Publications
ISSN (Online): 3107-538X
Vol. 02, Issue 06, November-December 2026

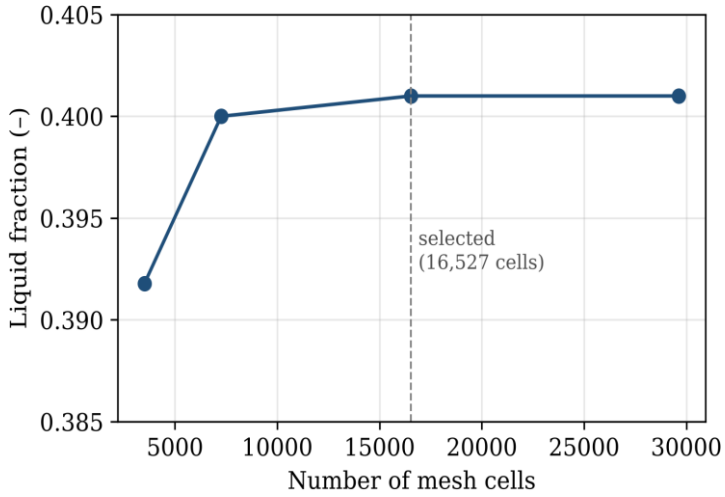


Figure 2: Liquid fraction predicted on the four meshes.

The model was validated against the measured melt-fraction history of Kamkari and Shokouhmand [17] for a single-fin enclosure with the same dimensions and wall temperature (Figure 3). Agreement is close throughout the charging period. The simulation is slightly ahead during the first minutes, which is consistent with the finite time needed by the experimental wall to reach its set temperature, whereas the model imposes 70 °C from $t = 0$.

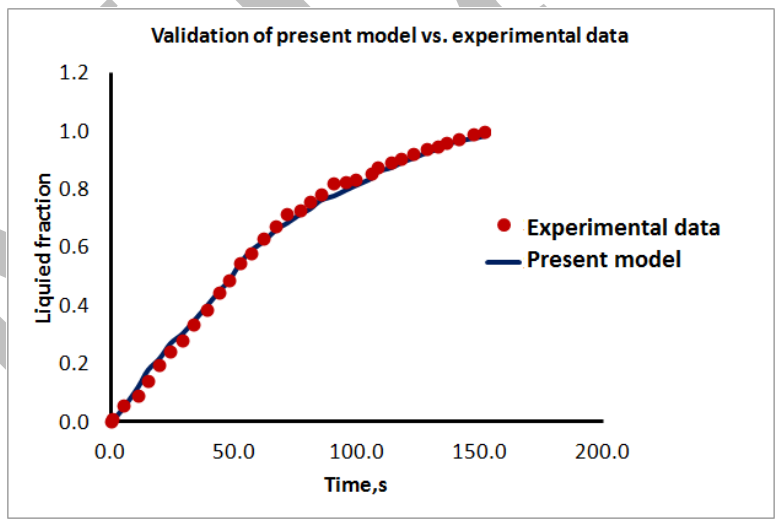


Figure 3: Validation of the model against the single-fin melting experiment of Kamkari and Shokouhmand [17].

3. SCALING AND CONDUCTION REFERENCE

Three dimensionless groups characterise the problem: the Stefan number $Ste = c_{p,l}(T_w - T_l)/L$, the Fourier number $Fo = \alpha t/L_c^2$ and the Rayleigh number based on the enclosure height. With the properties of Table 1, $Ste = 0.278$ and $\alpha = k_l/(\rho_l c_{p,l}) = 6.62 \times 10^{-8}$ m^2 s^{-1}. The diffusion time across the enclosure, L_c^2/α, is therefore about 630 min, and Fo reaches only 0.28 at the end of the 175 min simulation.

To quantify how much of the melting is due to convection, the simulations are compared with a conduction-only reference: the one-phase Neumann solution for a semi-infinite solid at its melting point whose face is raised suddenly to T_w [28]. The melt front advances as

$$s(t) = 2\zeta\sqrt{\alpha t}, \quad \zeta e^{\zeta^2} erf(\zeta) = \frac{Ste}{\sqrt{\pi}} \tag{5}$$

which for $Ste = 0.278$ gives $\zeta = 0.357$. Because the heated wall spans the full height, the conduction-only melt fraction of the enclosure is $\lambda_{cond} = s/L_c$. It equals 0.169, 0.238, 0.337 and 0.377 at 35, 70, 140 and 175 min, and complete melting by conduction alone would take $L_c^2/(4\zeta^2\alpha) \approx 1230$ min, i.e. about 20 h. The reference neglects the sensible heating of the initially subcooled solid and is therefore slightly optimistic, which makes the comparison conservative. The ratio

$$E = \frac{\lambda_{avg}}{\lambda_{cond}} \tag{6}$$

then measures the combined effect of natural convection and fin conduction relative to pure wall conduction; $E > 1$ indicates that the melt is gaining from the buoyant flow or from the fin.

4. RESULTS AND DISCUSSION

Liquid-fraction contours and velocity vectors are shown at 35, 70, 140 and 175 min. In the contours red is liquid, blue is solid and the narrow band of intermediate colours is the mushy zone. For reasons of post-processing, some panels display the heated wall on the left and others on the right; the captions state which, and the reflection does not alter the physics.

4.1. Enclosure without a fin

Without a fin (Figure 4), a continuous melt layer covers the heated wall after 35 min. It is already wedge-shaped, thin at the bottom and wide at the top, which shows that buoyant flow is redistributing heat even at this early time. By 70 min the upper part has melted across almost the entire width and the interface has an S-shape; by 140 min the liquid occupies the top of the enclosure and a band along the heated wall; and at 175 min the solid survives only as a wedge on the bottom wall, bounded above by a nearly horizontal interface.

Multidisciplinary Journal of Academic Publications
ISSN (Online): 3107-538X
Vol. 02, Issue 06, November-December 2026

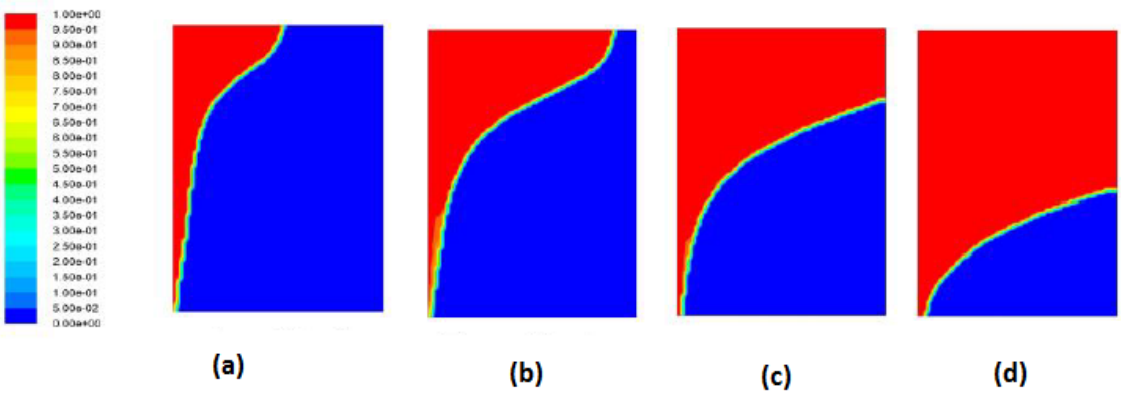


Figure 4: Liquid-fraction contours without a fin at (a) 35, (b) 70, (c) 140 and (d) 175 min (heated wall on the left).

The velocity field (Figure 5) explains this sequence. At 35 min the motion is confined to a thin boundary layer rising along the wall. At 70 min a single clockwise cell fills the melt: hot liquid ascends along the wall, turns under the top wall and descends along the inclined interface, losing heat to the solid. As the melt grows, the upper part of the cavity becomes almost stagnant because the warmest liquid accumulates there in a stable, stratified layer. At 175 min the active circulation is reduced to a shallow cell above the residual solid. The melting of the lower region therefore depends on fluid that has already given up much of its heat higher in the enclosure, which is why it is the slowest part of the process.

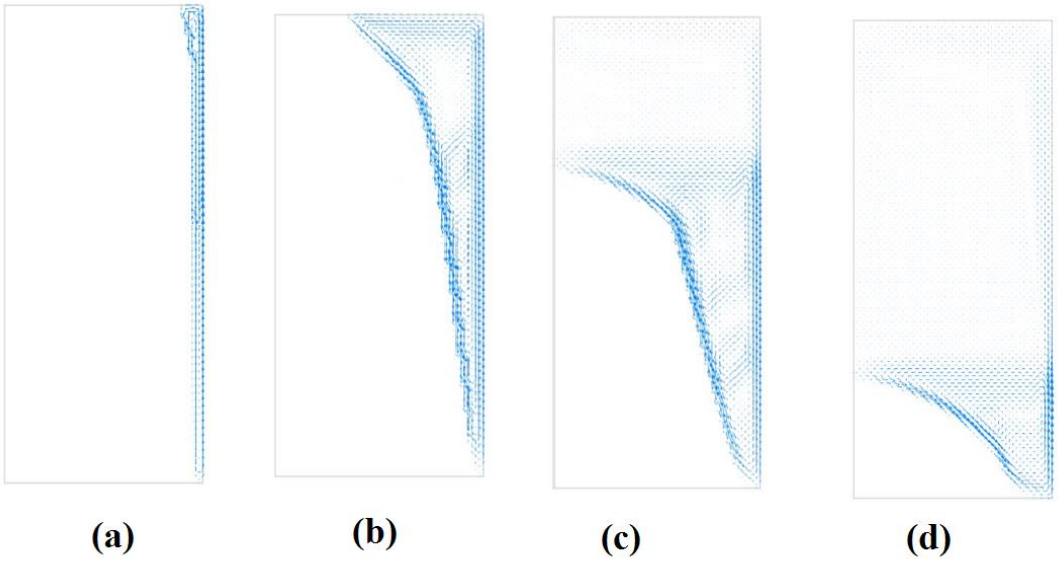


Figure 5: Velocity vectors without a fin at (a) 35, (b) 70, (c) 140 and (d) 175 min (heated wall on the right).

4.2. Fin at mid-height ($d_f = 0.50$)

With the fin at mid-height (Figure 6), the 35 min contour shows a thin, almost uniform melt layer along the wall and around the whole fin, indicating conduction-controlled melting from an enlarged heated surface. At 70 min the melt has expanded markedly both above and below the fin: a lobe of liquid extends beyond the fin tip in the upper half, and the melt layer in the lower half is thicker than at the same height without a fin. At 140 min solid remains only in the upper corner opposite the heated wall and in a thin strip at the bottom, and at 175 min the PCM is practically fully molten.

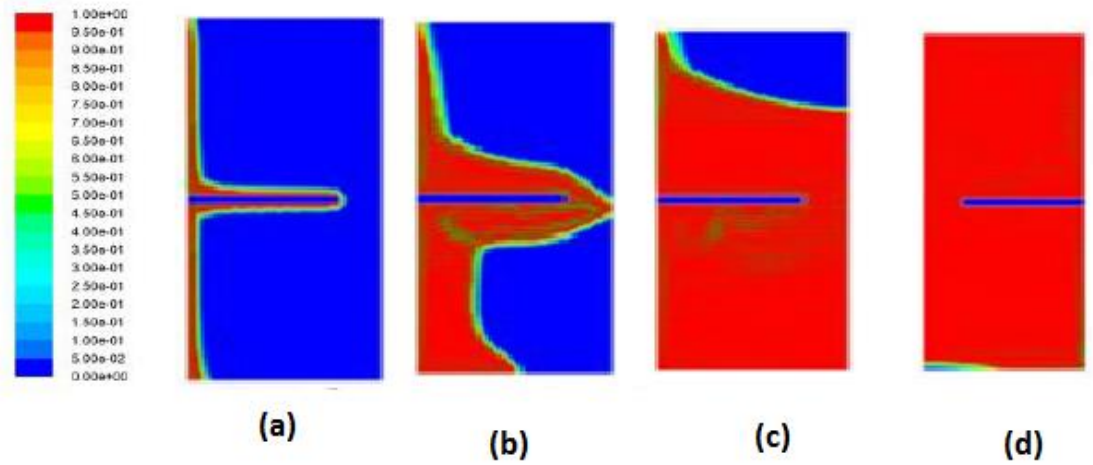


Figure 6: Liquid-fraction contours with a fin at $d_f = 0.50$ at (a) 35, (b) 70, (c) 140 and (d) 175 min (heated wall on the left).

The velocity vectors (Figure 7) reveal the reason. The fin interrupts the wall boundary layer, so two separate boundary layers develop, one below and one above it. By 70 min they feed two counter-rotating convection cells. The lower cell is bounded above by the fin, which prevents its warm liquid from escaping upwards; the fluid travels outward along the underside of the fin, descends along the interface and keeps eroding the solid in the lower half. The upper cell is driven by the wall above the fin and by a plume rising from the fin tip. As charging continues, the upper cell weakens as its liquid stratifies, but the lower cell remains active until little solid is left. The mid-height fin thus does more than add area: it creates a second, independent circulation in the region that the single cell of the no-fin case reaches last.

Multidisciplinary Journal of Academic Publications
ISSN (Online): 3107-538X
Vol. 02, Issue 06, November-December 2026

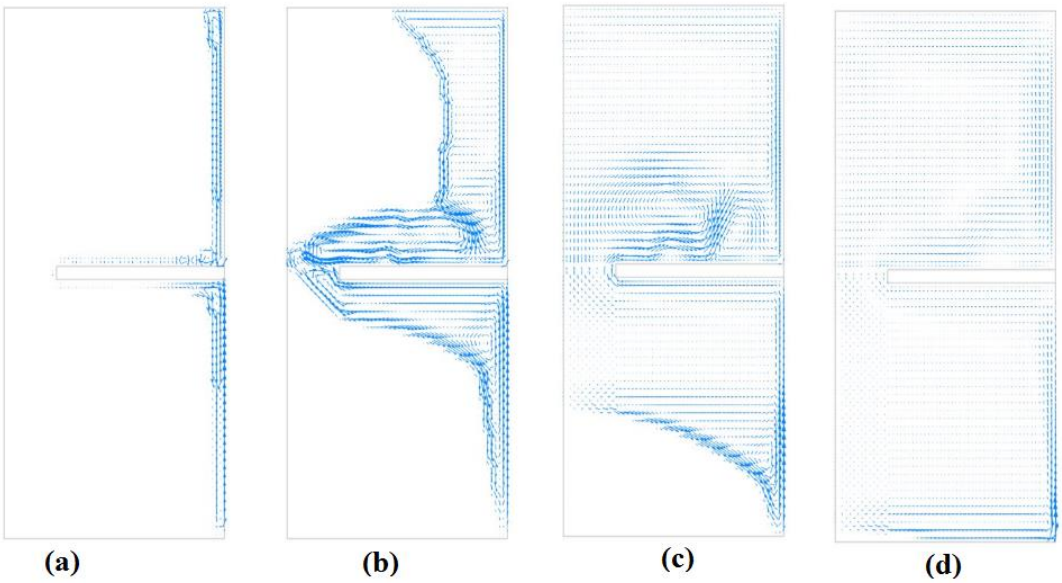


Figure 7: Velocity vectors with a fin at d_f = 0.50 at (a) 35, (b) 70, (c) 140 and (d) 175 min (heated wall on the right).

4.3. Fin in the upper part (d_f = 0.80)

When the fin is placed at d_f = 0.80 (Figure 8), the early melt again follows the wall and the fin. By 70 min the region above the fin and the top of the cavity have melted, and by 140 min about the upper 60% of the enclosure is liquid. At 175 min a sizeable lens of solid remains in the lower corner opposite the heated wall, clearly larger than in the mid-height case.

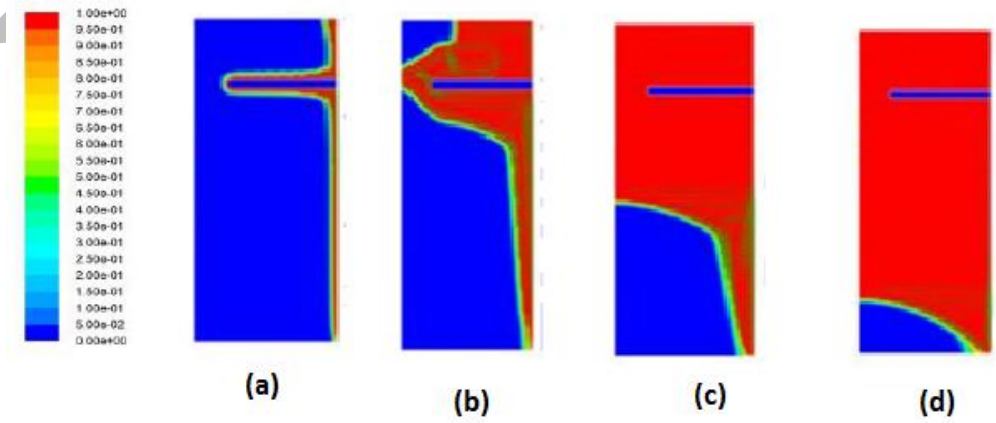


Figure 8: Liquid-fraction contours with a fin at d_f = 0.80 at (a) 35, (b) 70, (c) 140 and (d) 175 min (heated wall on the right).

Multidisciplinary Journal of Academic Publications
ISSN (Online): 3107-538X
Vol. 02, Issue 06, November-December 2026

The flow field (Figure 9) shows a small, vigorous cell above the fin at 70 min, but this region is shallow and quickly fills with hot liquid. The main circulation lies below the fin: liquid rises along the wall, is deflected by the fin underside and returns along the interface. At 140 and 175 min the region above the fin and much of the melt beneath it are nearly stagnant, and the active flow is restricted to a thin layer near the wall and the lower interface. Heat conducted through a high fin is therefore delivered largely to fluid that is already hot and stably stratified, and only a small part of it reaches the solid at the bottom.

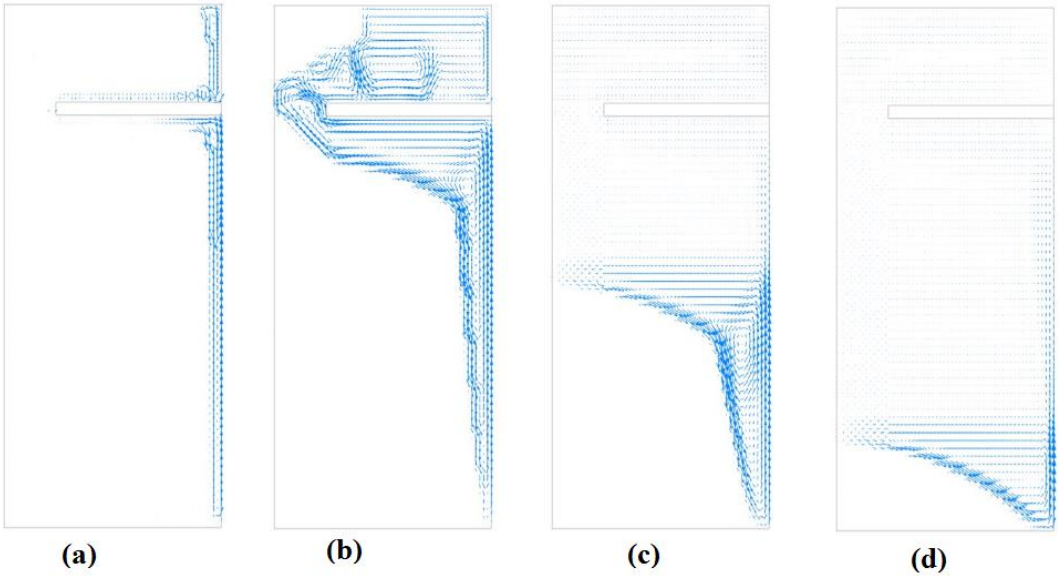


Figure 9: Velocity vectors with a fin at d_f = 0.80 at (a) 35, (b) 70, (c) 140 and (d) 175 min.

4.4. Melt fraction, charging time and stored energy

The melt fraction of each case was obtained from the contour plots by mapping each pixel of the PCM region onto the colour scale and averaging; the fin area was excluded. The resulting values (Table 3) carry an estimated uncertainty of about ±0.03, which is largest at 35 min when the melt layers are only a few pixels thick.

Table 3: Area-averaged liquid fraction, conduction reference and enhancement ratio *E*.

t (min)	*Fo*	λ_{cond}	No fin	d_f = 0.50	d_f = 0.80	*E* (no fin / 0.50 / 0.80)
35	0.056	0.169	0.19	0.11	0.11	1.15 / 0.66 / 0.64
70	0.111	0.238	0.32	0.38	0.36	1.34 / 1.61 / 1.50
140	0.222	0.337	0.45	0.83	0.65	1.34 / 2.45 / 1.94
175	0.278	0.377	0.71	0.99	0.90	1.87 / 2.62 / 2.38

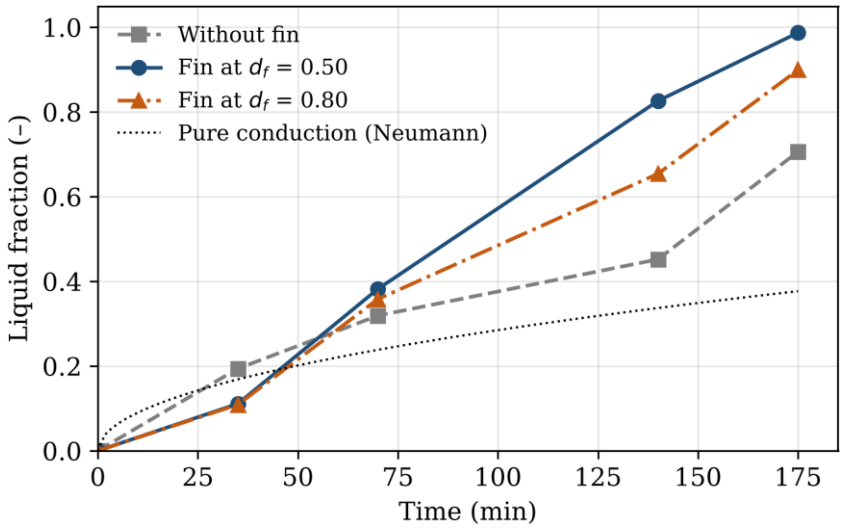


Figure 10: Evolution of the liquid fraction for the three configurations compared with the Neumann conduction reference.

Figure 10 shows that from 70 min onwards both finned enclosures melt faster than the plain enclosure and that the mid-height fin is clearly superior. Linear interpolation between the sampled instants gives the times needed to melt half and 70% of the PCM. Without a fin $t_{50} \approx 147$ min and $t_{70} \approx 174$ min; with the fin at $d_f = 0.50$ these become about 89 and 120 min (reductions of 40% and 31%), and with the fin at $d_f = 0.80$ about 104 and 147 min (29% and 16%). The upper fin therefore delivers roughly half the benefit of the mid-height fin for an identical amount of fin material. The fin displaces 3.3% of the PCM, so the latent capacity of the finned enclosures is about 1021 kJ per metre depth against 1056 kJ m^{-1} without a fin. Even so, the latent heat stored after 175 min is about 1008 kJ m^{-1} with the mid-height fin and 918 kJ m^{-1} with the upper fin, compared with 745 kJ m^{-1} without a fin. The corresponding mean latent charging rates over the period are about 96, 87 and 71 W m^{-1}, i.e. 35% and 23% higher than for the plain enclosure.

The enhancement ratio (Figure 11) separates the regimes. For the plain enclosure E is already 1.15 at 35 min and grows to 1.87 at 175 min, confirming that natural convection carries a growing share of the heat once a melt layer exists, in line with the scaling picture of Jany and Bejan [16]. For the finned enclosures E rises steeply between 35 and 140 min, to 2.45 for $d_f = 0.50$ and 1.94 for $d_f = 0.80$, and the gap between the two fin heights opens precisely when stratification begins to dominate the upper half. The finned values below unity at 35 min are not physically expected, since the fin only adds heated area; they are attributed to the limited resolution of the thin early melt layers in the images and should be verified with solver-integrated values.

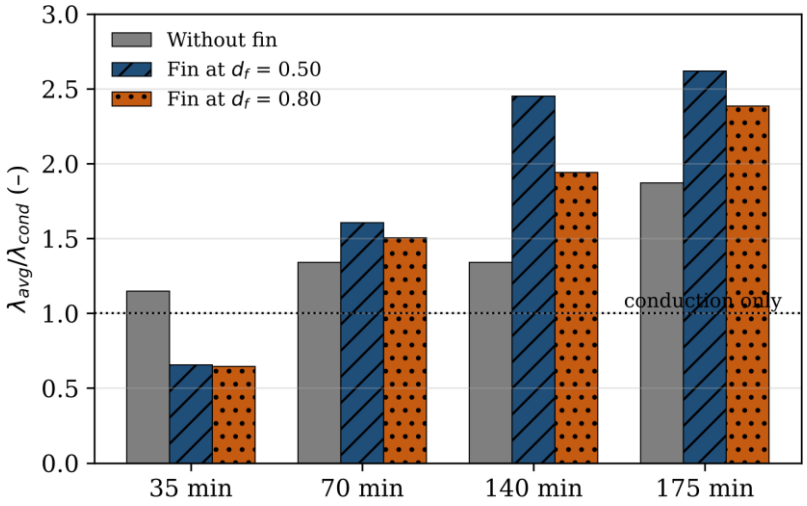


Figure 11: Enhancement ratio $E = \lambda_{avg}/\lambda_{cond}$ for the three configurations.

4.5. Mechanism and design implications

Taken together, the contours, velocity fields and metrics describe three stages. In the conduction-dominated start, the fin acts simply as additional heated surface and its height has little influence. In the intermediate stage, buoyant flow carries the heat upward and the enclosure melts from the top down; a fin at mid-height splits the melt into two cells and keeps a strong circulation in the lower half. In the late stage, the upper melt is stably stratified and nearly motionless, so heat supplied there contributes little to melting; the residual solid near the bottom then controls the charging time. A fin located high in the enclosure feeds heat into this stratified layer and also forces the main circulation to pass beneath it, which explains why the solid left at 175 min is several times larger than with the mid-height fin.

Additional runs with the fin very close to the bottom ($d_f = 0.05$) and to the top ($d_f = 0.95$) support this interpretation. Near the bottom, the fin rapidly melted the lower part of the enclosure but left a large solid region in the upper half far from the wall, so that the interface resembled the plain-enclosure case. Near the top, the opposite occurred: the top region melted completely while the bottom remained largely solid. The best location therefore balances the conduction path provided by the fin against the region already served by the buoyant flow. For a single fin on a side-heated wall this points to the lower half, typically near mid-height, where the fin both supplies heat to the region that convection reaches last and creates an independent convection cell there. These findings are consistent with the trends reported by Huang et al. [22] and with the early-stage behaviour documented in our companion study [23].

4.6. Limitations

The simulations are two-dimensional and neglect the volume change on melting and any heat loss from the nominally adiabatic walls. Only two fin heights were simulated over the full period, and the quantitative metrics are derived from contour images sampled at four instants, so the interpolated t_{50} and t_{70} values should be regarded as indicative. Extending the study to a finer range of d_f, exporting solver-integrated liquid fraction and wall heat flux, and including the discharging process are natural next steps.

5. CONCLUSIONS

The long-duration melting of lauric acid in a 50 mm × 120 mm enclosure heated from one side wall was simulated with a validated enthalpy–porosity model for no fin and a single horizontal fin at d_f = 0.50 and 0.80. The main findings are:

(1) Melting proceeds from a short conduction-controlled stage to convection-dominated melting in which the melt stratifies and the enclosure melts from the top downward; the last solid is always found at the bottom, away from the heated wall.

(2) A mid-height fin interrupts the wall boundary layer and creates a second convection cell that keeps the lower half of the enclosure active. It melted about 99% of the PCM in 175 min, compared with about 90% for the upper fin and 71% without a fin.

(3) Relative to the plain enclosure, the times to 50% and 70% melting fell by about 40% and 31% with the mid-height fin and by about 29% and 16% with the upper fin, and the mean latent charging rate rose by about 35% and 23%, despite the 3.3% loss of PCM volume to the fin.

(4) Compared with a Neumann conduction reference, the melt fraction at 175 min was 2.6, 2.4 and 1.9 times the conduction-only value for d_f = 0.50, 0.80 and no fin, showing that convection and fin conduction together supply most of the charging.

(5) A fin placed high in the enclosure heats liquid that is already stably stratified. In side-heated stores, fins should be located so that they supply heat to the lower region that natural convection reaches last.

6. CREDIT AUTHORSHIP CONTRIBUTION STATEMENT

Amirraza: Conceptualization, Methodology, Software, Validation, Formal analysis, Investigation, Visualization, Writing – original draft. **Sachin Baraskar:** Conceptualization, Supervision, Resources, Writing – review & editing.

7. DECLARATION OF COMPETING INTEREST

The authors declare that they have no known competing financial interests or personal relationships that could have appeared to influence the work reported in this paper.

8. DATA AVAILABILITY

Data will be made available on request.

9. DECLARATION OF GENERATIVE AI AND AI-ASSISTED TECHNOLOGIES IN THE WRITING PROCESS

During the preparation of this work the authors used to improve the language and structure of the manuscript. After using this tool, the authors reviewed and edited the content as needed and take full responsibility for the content of the publication.

10. ACKNOWLEDGEMENTS

The authors thank the Department of Mechanical Engineering, Sri Satya Sai University of Technology & Medical Sciences, Sehore, for providing computational facilities. This research did not receive any specific grant from funding agencies in the public, commercial, or not-for-profit sectors.

11. REFERENCES

[1] A. Sharma, V.V. Tyagi, C.R. Chen, D. Buddhi, Review on thermal energy storage with phase change materials and applications, Renew. Sustain. Energy Rev. 13 (2009) 318–345.

[2] F. Agyenim, N. Hewitt, P. Eames, M. Smyth, A review of materials, heat transfer and phase change problem formulation for latent heat thermal energy storage systems (LHTESS), Renew. Sustain. Energy Rev. 14 (2010) 615–628.

[3] M. Kenisarin, K. Mahkamov, Solar energy storage using phase change materials, Renew. Sustain. Energy Rev. 11 (2007) 1913–1965.

[4] B. Zalba, J.M. Marín, L.F. Cabeza, H. Mehling, Review on thermal energy storage with phase change: materials, heat transfer analysis and applications, Appl. Therm. Eng. 23 (2003) 251–283.

[5] M.M. Farid, A.M. Khudhair, S.A.K. Razack, S. Al-Hallaj, A review on phase change energy storage: materials and applications, Energy Convers. Manag. 45 (2004) 1597–1615.

[6] L. Fan, J.M. Khodadadi, Thermal conductivity enhancement of phase change materials for thermal energy storage: a review, Renew. Sustain. Energy Rev. 15 (2011) 24–46.

[7] S. Jegadheeswaran, S.D. Pohekar, Performance enhancement in latent heat thermal storage system: a review, Renew. Sustain. Energy Rev. 13 (2009) 2225–2244.

[8] S. Rostami, M. Afrand, A. Shahsavar, M. Sheikholeslami, R. Kalbasi, S. Aghakhani, et al., A review of melting and freezing processes of PCM/nano-PCM and their application in energy storage, Energy 211 (2020) 118698.

[9] N.S. Dhaidan, J.M. Khodadadi, Improved performance of latent heat energy storage systems utilizing high thermal conductivity fins: a review, J. Renew. Sustain. Energy 9 (2017) 034103.

[10] M. Eslami, F. Khosravi, H.R. Fallah Kohan, Effects of fin parameters on performance of latent heat thermal energy storage systems: a comprehensive review, Sustain. Energy Technol. Assess. 47 (2021) 101449.

[11] Z.H. Low, et al., A review of fin application for latent heat thermal energy storage enhancement, J. Energy Storage (2024) 111157.

[12] N. Sharifi, T.L. Bergman, A. Faghri, Enhancement of PCM melting in enclosures with horizontally-finned internal surfaces, Int. J. Heat Mass Transf. 54 (2011) 4182–4192.

[13] U. Stritih, An experimental study of enhanced heat transfer in rectangular PCM thermal storage, Int. J. Heat Mass Transf. 47 (2004) 2841–2847.

[14] B. Kamkari, H. Shokouhmand, F. Bruno, Experimental investigation of the effect of inclination angle on convection-driven melting of phase change material in a rectangular enclosure, Int. J. Heat Mass Transf. 72 (2014) 186–200.

[15] C. Gau, R. Viskanta, Melting and solidification of a pure metal on a vertical wall, J. Heat Transf. 108 (1986) 174–181.

[16] P. Jany, A. Bejan, Scaling theory of melting with natural convection in an enclosure, Int. J. Heat Mass Transf. 31 (1988) 1221–1235.

[17] B. Kamkari, H. Shokouhmand, Experimental investigation of phase change material melting in rectangular enclosures with horizontal partial fins, Int. J. Heat Mass Transf. 78 (2014) 839–851.

[18] B. Kamkari, H.J. Amlashi, Numerical simulation and experimental verification of constrained melting of phase change material in inclined rectangular enclosures, Int. Commun. Heat Mass Transf. 88 (2017).

[19] X. Cao, Y. Yuan, B. Xiang, L. Sun, Z. Xingxing, Numerical investigation on optimal number of longitudinal fins in horizontal annular phase change unit at different wall temperatures, Energy Build. 158 (2018) 384–392.

[20] X. Cao, Y. Yuan, B. Xiang, F. Haghighat, Effect of natural convection on melting performance of eccentric horizontal shell and tube latent heat storage unit, Sustain. Cities Soc. 38 (2018) 571–581.

[21] C. Ji, Z. Qin, Z. Low, S. Dubey, F.H. Choo, F. Duan, Non-uniform heat transfer suppression to enhance PCM melting by angled fins, Appl. Therm. Eng. 129 (2018) 269–279.

[22] B. Huang, L.-L. Tian, Q.-H. Yu, X. Liu, Z.-G. Shen, Numerical analysis of melting process in a rectangular enclosure with different fin locations, Energies 14 (2021) 4091.

[23] Amirraza, S. Baraskar, Numerical analysis of fin position effects on PCM melting and natural convection in a rectangular enclosure.

[24] V.R. Voller, C. Prakash, A fixed grid numerical modelling methodology for convection-diffusion mushy region phase-change problems, Int. J. Heat Mass Transf. 30 (1987) 1709–1719.

[25] A.D. Brent, V.R. Voller, K.J. Reid, Enthalpy-porosity technique for modeling convection-diffusion phase change: application to the melting of a pure metal, Numer. Heat Transf. 13 (1988) 297–318.

[26] ANSYS Inc., ANSYS Fluent Theory Guide, Release 15.0, Canonsburg, PA, 2013.

[27] S.V. Patankar, Numerical Heat Transfer and Fluid Flow, Hemisphere, Washington, DC, 1980.

[28] H.S. Carslaw, J.C. Jaeger, Conduction of Heat in Solids, 2nd ed., Oxford University Press, Oxford, 1959.

MJAP